Soft Matter

PAPER

View Article Online
View Journal | View Issue

Cite this: *Soft Matter*, 2016, 12, 4725

Rupture and recoil of bent-core liquid crystal filaments†

S. M. Salili,[a] T. Ostapenko,‡[b] O. Kress,‡[a] C. Bailey,[c] W. Weissflog,[d] K. Harth,[b] A. Eremin,[b] R. Stannarius*[b] and A. Jákli*[a]

Received 3rd February 2016,
Accepted 7th April 2016

DOI: 10.1039/c6sm00290k

www.rsc.org/softmatter

The recoil process of free-standing liquid crystal filaments is investigated experimentally and theoretically. We focus on two aspects, the contraction speed of the filament and a spontaneously formed undulation instability. At the moment of rupture, the filaments buckle similarly to the classical Euler buckling of elastic rods. The tip velocity decays with decreasing filament length. The wavelength of buckling affinely decreases with the retracting filament tip. The energy gain related to the decrease of the total length and surface area of the filaments is mainly dissipated by layer rearrangements during thickening of the fibre. A flow back into the meniscus is relevant only in the final stage of the recoil process. We introduce a model for the quantitative description of the filament retraction speed. The dynamics of this recoil behaviour may find relevance as a model for biology-related filaments.

Introduction

Filamentous materials hold promise for an entirely new class of artificial muscles and/or strain sensors due to their fascinating mechanical, electro-mechanical, optical and electro-optical properties. Dynamic buckling and recoil mechanisms of elastic materials have been studied in materials ranging from solids[1] to rubbers[2] and even to non-Newtonian fluids.[3–8] When the axial compression of a straight beam exceeds a critical value, a dynamic buckling instability initiates – as noted first by Euler[9] – with a characteristic wavelength.[1,10,11] The threshold character of this phenomenon may be the first practical example of a critical bifurcation of the solution of a differential equation. Apart from that, interesting dynamic properties are found when the critical stress is exceeded.[12] Dynamic instabilities can also be triggered in rotationally forced filament rubbers[13,14] and in an elastic rubber band submerged in a viscous fluid,[2] or during the extrusion of a rod into a viscous fluid.[15]

Some viscoelastic materials can easily form free-standing filaments and can be stabilized by hardening induced by cooling, solvent evaporation (as in spider silk[16]), or polymerization. The dynamic buckling instability of filaments of non-Newtonian fluids is a phenomenon replete with complexity. The degree of this complexity increases when a dynamic buckling instability becomes responsible for the recoil of a fluid filament when one end is broken free from its structural support. Such processes have tremendous importance in diverse biophysical phenomena, such as the viscoelastic properties of muscle fibres in the physiologically relevant regime, which have been studied only recently.[13,14,17–19]

Newtonian fluids show elastic responses only at free surfaces due to surface tension. In the filament form, they experience a Plateau–Rayleigh instability when their length L is larger than their perimeter, $2\pi R$.[20,21] Fluids with one- or two-dimensional internal molecular order, such as columnar and some smectic liquid crystals, may overcome the P–R instability to form stable, free-standing liquid filaments.[22] In particular, stable filaments can be formed by achiral bent-core liquid crystals with nano-scale modulated smectic and columnar (B7) phases. They can be considered as 1-D fluid structures exhibiting high slenderness ratios greater than 10 000.[23–28] These bent-core filaments have a fascinating structure. Recently, we described the formation of chiral nanostructures observed in these filaments,[27] which are believed to contribute to their viscoelastic behaviour.[22]

Here, we present our experimental methods, results and analysis of the rupture and recoil properties of several bent-core liquid crystal filaments, anticipating that they may serve as a model system for complex biological fibres.

[a] *Chemical Physics Interdisciplinary Program and Liquid Crystal Institute, Kent State University, Kent, OH 44242, USA. E-mail: ajakli@kent.edu*
[b] *Institute of Experimental Physics, Otto von Guericke University, Universitätsplatz 2, 39106 Magdeburg, Germany. E-mail: ralf.stannarius@ovgu.de*
[c] *Leidos, 3745 Pentagon Blvd., Beavercreek, OH 45431, USA*
[d] *Martin Luther University Halle-Wittenberg, Department of Chemistry, Physical Chemistry, von-Danckelmann-Platz 4, 06120 Halle, Germany*

† Electronic supplementary information (ESI) available. See DOI: 10.1039/c6sm00290k

‡ Current affiliation: Max Planck Institute for Dynamics and Self-Organization (MPIDS), Am Faßberg 17, 37077 Göttingen, Germany.

Experimental

For our studies, we chose the n = 7 and n = 16 homologues of 2-nitro-1,3-phenylene bis[4-(4-n alkyloxy phenylimino methyl)-benzoates], which are the prototypical B7 materials where the peculiar chiral superstructures were first observed[29] [see Fig. 1(a)] because they form the most stable bent-core filaments discovered so far. Both the n = 7 (N7) and n = 16 (N16) materials have a B7 phase with a broad temperature range between $T_{I\text{-}B7}$ = 174 °C and $T_{B7\text{-}Cr}$ = 85 °C. In this phase, the materials have a monoclinic, 2-D lattice with parameters a, b and ϕ, where a is the smectic layer spacing, b is the periodicity of the layer undulation and ϕ is the angle between a and b. These parameters are nearly temperature independent in the bulk. For example, at 150 °C, they are a = 3.43 nm, b = 9.0 nm, and ϕ = 85° for N7, and a = 4.7 nm, b = 15.6 nm, and ϕ = 81.6° for N16. Recent cryo-TEM experiments show that these materials have a strongly modulated layer structure, where there are half layer step discontinuities at the boundaries of the splay domains,[30] which resemble columnar structures.[31,32]

A motorized and temperature-controlled setup [Fig. 1(b)], in which 1 mm diameter glass capillaries with fused tips were used to manipulate the filaments, was built in our lab. This apparatus provides motion in three orthogonal directions so that the positions of the two tips can be adjusted with respect to each other and moved apart to initially draw and later stretch the filaments. The filaments were formed a few degrees below the isotropic-B7 phase transition, with diameters between 4 μm and 7 μm. A high-speed CCD camera (Phantom v211) was used to record video at frame rates between 1900 and 6000 frames per second. It was mounted onto a Nikon inverted optical microscope on which the pulling device was placed for observation.

Filament ruptures were initiated both mechanically and thermally. In order to induce a mechanical rupture, the fibre length was suddenly increased. This was repeated at different shear rates for several fibres. Thermal rupture was initiated by heating the air surrounding the fibre at 20 K min^{-1} until one end reached the clearing temperature. Typically, the same end ruptured each time due to one of the glass capillaries being closer to the heating element than the other. Before the ruptures were triggered, the filaments were pulled to a length not longer than 2 mm at constant temperature.

After rupture, the filaments retract by forming a buckling structure as illustrated schematically in Fig. 1(c) and by snapshots taken at short time intervals using the fast camera in Fig. 2(a) and (b) for thermal and mechanical ruptures, respectively. The images show only part of the filaments while the video in the ESI† shows the entire filaments. It should be noted that in Fig. 2(b), the filament ruptured in the middle. Although the still frames only allow a two-dimensional analysis as illustrated in Fig. 1(c), a close observation of details of the video footage (out of focus displacements) reveals three-dimensional recoiling.

One immediately observes a relation between the undulation structure and the filament material displacement: does the undulation travel like an elastic wave along the filament or are the undulations fixed to the material?

In Fig. 2(c) and (d), the images were stretched to adjust for the filament tip displacement after each time step. The images show that the undulations stay in essentially the same positions, with only a slight shift towards the tip of the filament. In addition,

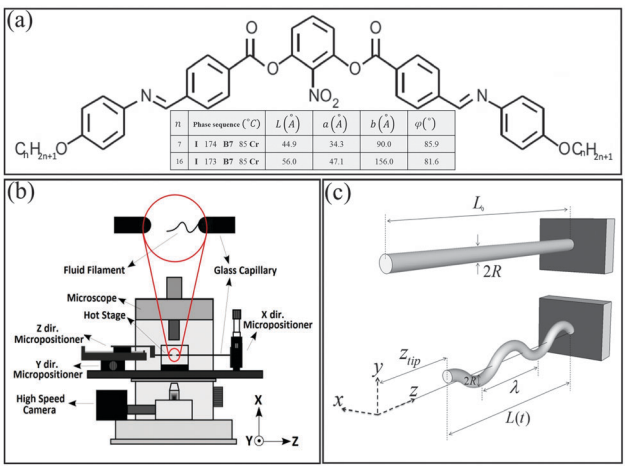

Fig. 1 Molecular structure, experimental setup and filament geometry. (a) Molecular structure with phase sequences and parameters; (b) schematic of the experimental setup. (c) Top: Straight filament before rupture; bottom: recoiling filament with the coordinate system and parameters used in text. Note, in reality, the buckled filaments are less regular.

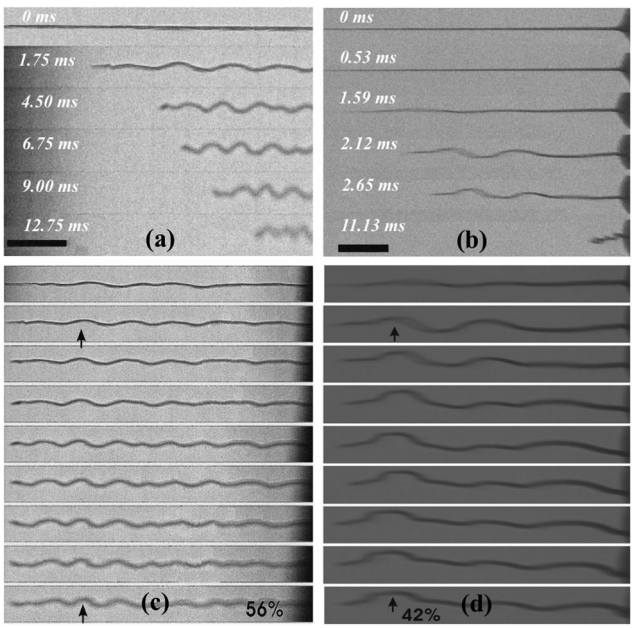

Fig. 2 Snapshots of recoiling filaments. (a) Thermal initiation at T = 165 °C for N16; (b) mechanical initiation at 170 °C for N7. Scale bars indicate 200 μm length. (c and d) The individual frames have been stretched to a fixed total length of the filament images. We see that the undulations are nearly affinely transformed with the retraction of the filament tip. The wavelength of the undulations decreases, and their amplitude increases. See text for details. (c) N16, T = 165 °C, time steps between snapshots are 1 ms; (d) N7, T = 170 °C, time steps between snapshots are 0.53 ms. The percentages shown in the last frames of (c) and (d) indicate the length of the filament in the last frame, compared to the initial length.

new, smaller wavelength undulations appear at later stages. This leads to the conclusion that the undulations remain essentially fixed to the material, *i.e.* the contraction is nearly uniform along the filament. While the tip collects some filament material during rupture, the main influence on filament retraction comes from a global, uniform shortening of the filament requiring the local radius to increase. This is accompanied by a growth of the undulation amplitudes and the formation of additional undulations. The retraction of the material into the meniscus seems to be of minor importance; otherwise, the wave structures would move to the right, approaching the fixed edge (meniscus) in the images of Fig. 2(c) and (d).

To understand the quantitative relation between the tip movement and the length of the filament, we normalized the arc length of the projected filament shown in Fig. 2(c) and plotted it *versus* time in Fig. 3(a). The open circles show the straight relative distance from the filament's tip to its base ($L(t)/L_0$), while the filled circles represent the filament's total (arc) relative length. The reduction of the total length is smaller than the reduction of the end-to-end length by approximately 10%. Of course, the video shows only a 2D projection of the buckled and coiled filament, thus underestimating the remaining filament length. Assuming a three-dimensional undulation, one can estimate that the actual length reduction amounts to about 80% of the observed tip motion.

The initial wavelength of the buckling pattern was observed to be about 150–200 μm for both materials, decreasing with time proportional to the length $L(t)$ of the filament. For this reason (and based on our analysis described below in Discussion), we have fitted the data to the equation $\lambda(t) = \frac{\lambda(0)}{(1+\beta t)^2}$, where β is given in eqn (7). The best fits to this function are shown in Fig. 3(b). This holds for both rupture methods and is a direct consequence of the observed affine filament deformation seen in Fig. 2(c) and (d).

The time dependence of the displacement, $z_{tip}(t) = L_0 - L(t)$, of the endpoints of recoiling filaments is shown in Fig. 4. Fig. 4(a) and (b) show the time dependence for several temperatures when the rupture was initiated thermally. Fig. 4(a) shows $z_{tip}(t)$ of two $L_0 \sim 1.9$ mm length N7 filaments ruptured at 165 °C and 170 °C. Fig. 4(b) depicts $z_{tip}(t)$ of two N16 filaments ruptured at 160 °C (L_0 = 1.1 mm) and 165 °C (L_0 = 1.5 mm). One sees that the relative displacement increases quickly at the beginning, then slows down as $z_{tip}/L_0 \sim 1$ is approached. The speed of recoil depends on the temperature of the filament at the moment of rupture.

Since the temperature of the filament during the thermally induced rupture process is not uniform, we also tested the mechanical rupture at constant temperatures. The time dependences of the relative displacements at pulling speeds of 1.1, 1.3, 1.7 and 1.9 mm s^{-1} are shown in Fig. 4(c) for N7, and Fig. 4(d) for N16. One sees qualitatively similar behaviour in the thermally and mechanically initiated rupture processes, indicating that the temperature inhomogeneity might be negligible. The rate of recoil correlates to the pulling speed (faster speed–quicker retraction).

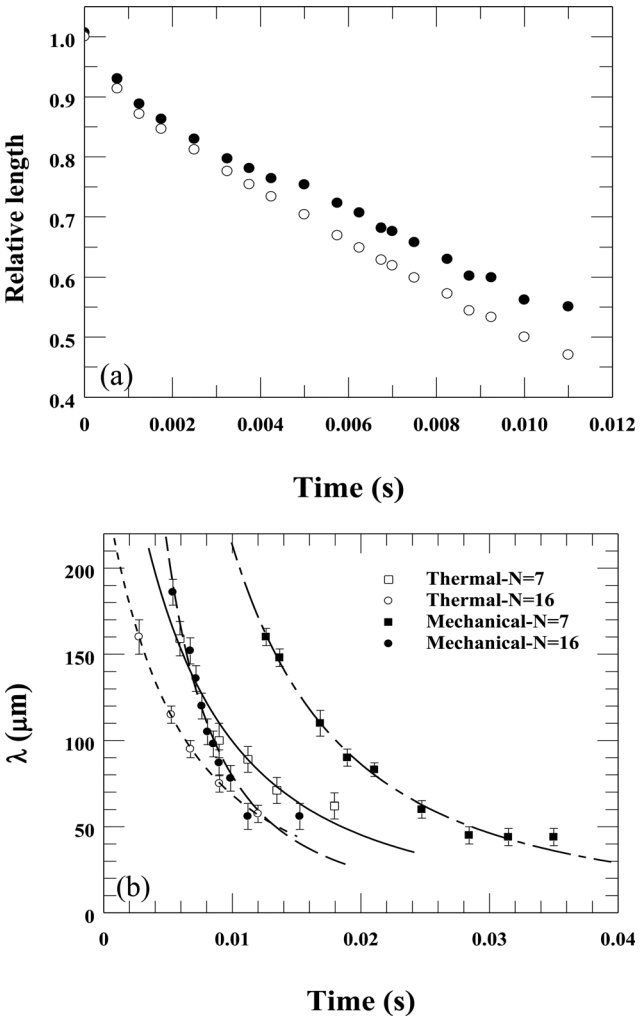

Fig. 3 Time dependences of the relative length and the dominant wavelength ($\lambda(t)$) of the undulated filament during recoil. (a) Reduction of the distance between the tip and the base of the filament (open circles) and reduction of the actual length (filled circles) assuming a 2D shape. (b) $\lambda(t)$ of filaments formed at 170 °C. Ruptures induced mechanically (filled symbols) occurred when the filament was stretched near the minimum shearing speed threshold of 1.1 mm s^{-1}. Thermal rupture (open symbols) was initiated as described earlier in this section at 165 °C. Squares: N7; circles: N16. The data at small times have larger errors due to the low amplitudes involved. The fit parameters for mechanically induced recoils are λ_0 = 1.2 mm (1.5 mm) and β = 134 s^{-1} (331 s^{-1}) for N7 (N16), and the thermally induced processes are λ_0 = 0.37 mm (0.25 mm) and β = 93 s^{-1} (91 s^{-1}) for N7 (N16).

Discussion

The above experiments show that the ruptures start with a visually observable buckling, similarly to the classic Euler buckling of a rod due to axial load.[9] In order to quantify this rupture behaviour, we consider the dynamic equation of lateral displacement $\xi(z,t)$ of a straight elastic beam under an applied longitudinal force T, which is

$$\rho A\ddot{\xi} + T\xi'' + EI\xi^{(iv)} = 0 \qquad (1)$$

where $\ddot{\xi} = \partial^2\xi/\partial t^2$, $\xi'' = \partial^2\xi/\partial z^2$, ρ is the mass density; $A = R^2\pi$ is the cross-sectional area of the filament with radius R; E is the

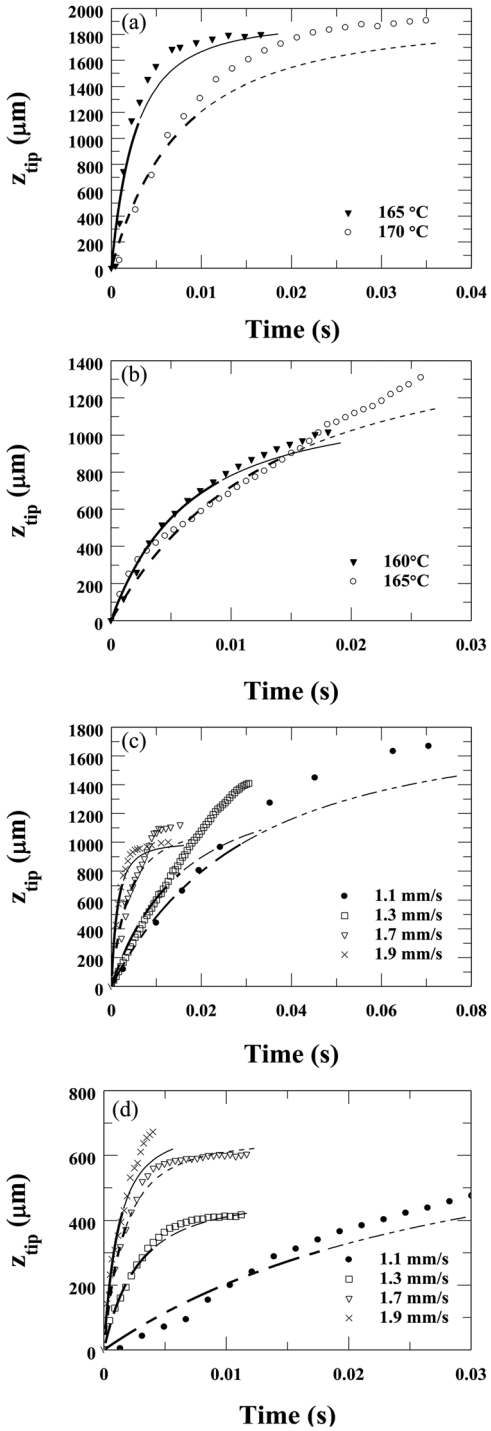

Fig. 4 Time dependences of z_{tip} of filaments after ruptures. (a and b) Thermally initiated ruptures at several temperatures for N7 (a) and N16 (b). (c and d) Mechanically initiated ruptures by fast pulling at various speeds at 165 °C for N7 (c) and N16 (d). Lines are best fits to equation $z_{tip} = L_0[1 - 1/(1 + \beta t)^2]$, based on eqn (8) derived in Discussion. In this equation L_0 is the initial length of the filament. Thick lines correspond to the range where the fit was obtained, thin lines show how they deviate from the data outside the fit range. For all fits, the lengths of the fibres were constant corresponding to the measured values. The fitted relaxation rate β values are the following: (a) β(165 °C) = 185 s^{-1}, β(170 °C) = 66 s^{-1}; (b) β(160 °C) = 78 s^{-1}, β(165 °C) = 39 s^{-1}; (c) β(1.1 mm s^{-1}) = 17 s^{-1}; β(1.3 mm s^{-1}) = 33 s^{-1}; β(1.7 mm s^{-1}) = 131 s^{-1}; β(1.9 mm s^{-1}) = 351 s^{-1}; (d) β(1.1 mm s^{-1}) = 19 s^{-1}; β(1.3 mm s^{-1}) = 182 s^{-1}; β(1.7 mm s^{-1}) = 306 s^{-1}; β(1.9 mm s^{-1}) = 418 s^{-1}.

Young's modulus, and $I = \pi R^4/4$ is the moment of inertia of the area. As shown for elastic rods,[1] the stability analysis of eqn (1) for a constant force T reveals the wavelength λ_0 and the growth rate τ^{-1} of the fastest growing mode to be:

$$\lambda_0 = \pi R^2 \sqrt{2\pi E/T} \quad (2)$$

$$\tau^{-1} = T \Big/ \left(\pi R^3 \sqrt{\rho E}\right) \quad (3)$$

In our system, the axial force is the tension of the filament that becomes unbalanced by the rupture, leading to buckling. Approximating the tension by $T \sim \sigma \cdot 2\pi R$, where $\sigma \sim 0.02$ N m^{-1} is the surface tension at a LC/air interface, we can express the bulk modulus E from eqn (2) as $E = \sigma\lambda_0^2/(\pi^2 R^3)$. With the measured $\lambda_0 \sim 200$ μm and $R \sim 3$ μm, this gives $E \sim 2.7$ MPa, which is within the order of magnitude of the typical layer compression modulus of smectic materials. Substituting this value into eqn (3), with $\rho \sim 10^3$ kg m^{-3}, we get $\tau^{-1} > 10^4$ s^{-1}. This is faster than the frame rate used by our camera, but we see from Fig. 2 that the growth of this mode took far less than a millisecond.

The snapshots of the recoil (Fig. 2) show that once buckling occurred, the number of waves n_w remained constant during the recoil process (in examples of Fig. 2, $n_w \cong 4$ for N16 and 3 for N7). This is consistent with the observation that the wavelength decreases during recoil as $\lambda(t) = L(t)/n_w$ (Fig. 3(b)).

The dynamics of the shape transformation is driven by the reduction of surface energy. Thus, it is insightful to estimate the amount of surface energy that is converted into kinetic energy. We start with an analysis similar to that developed to describe the propagation of the rim of bursting thin fluid films. The model of Taylor[33] and Culick[34] is based on the assumption that the moving edge of bursting films collects all the retracting material. This is fulfilled in good approximation for low viscosity (soap) films. For viscous sheets, a global thickening as in our experiments is a common feature.[35] For the filaments, we assume (and our observations support) that they contract uniformly, and only a small portion of the material of the retracting structure is collected in the tip.

The local velocity $v(z)$ along the filament axis is in good approximation proportional to the distance z from the filament base (meniscus). This yields $v(z) = v_{tip}z/L$ and a kinetic energy $E_{kin} = m{v_{tip}}^2/6$, where m is the filament mass. If we neglect the small frontal area of the filament, the surface area is

$$A = 2\pi RL = 2(\pi VL)^{1/2} = 2(\pi V(L_0 - z_{tip}))^{1/2}. \quad (4)$$

Here, V is the filament volume, which is approximated as constant (no material flows into the meniscus). Under the assumption that all surface energy from the reduction of the filament surface area A is converted into kinetic energy, one obtains

$$v_{tip} = (12\sigma/m)^{1/2}(\pi V)^{1/4}({L_0}^{1/2} - (L_0 - z_{tip})^{1/2})^{1/2}. \quad (5)$$

From this equation one can estimate that tip velocities of the order of several m s^{-1} should be reached when the energy conversion was complete. Experimentally, the tip velocities barely exceed 0.3 m s^{-1} suggesting that only a small portion of the surface energy, less than one percent, is converted into kinetic energy.

The majority is dissipated and a small part may be stored in elastic energies of the filament interior. This is in sharp contrast to the ratio of the kinetic and dissipated energies found for soap films, which are roughly equal. The dissipation of about one half of the surface energy in bursting soap films[33,34] is related to the impact of the rim material that moves at constant velocity on the film at rest. In that situation, the momentum balance requires the loss of mechanical energy, irrespective of the nature and details of the dissipative processes. This does not apply in our filaments, where no discontinuities in the velocity field are involved.

We assume that this difference is related to the more complex inner structure of the filaments,[36,37] which requires a greater level of reorganization of the internal layer arrangement than in more commonly studied soap films or smectic films.

In the experiment, we find that the filament tip initially moves with nearly constant speed (see Fig. 4), and the above estimation shows that the kinetic energy is in first approximation negligible with respect to the released surface energy. Thus, we can make the approximating assumption that after a short transient, all surface energy is dissipated. The dissipation term can be sought for an energy necessary to form new layers on the filament surface. This energy cannot be retrieved again when the filament thins. Thickening of the filament requires permeation flow across the smectic layers. To describe it, it is reasonable to introduce a viscous term that relates the layer formation process with a viscous coefficient γ. The relation between the growth rate $\dot{n}$ of new layers and the pressure in the corresponding filament segment is $p_\mathrm{d} = \frac{2\pi R\delta}{\pi R^2}\dot{n}\gamma$, where δ is the thickness of a single layer, n is the number of smectic layers, $A_0 = \pi R^2$ is the filament cross-section, and γ is a new material parameter, which has the unit of a viscosity. With $\dot{n}\delta = \dot{R}$, one obtains $p_d = 2\gamma\dot{R}/R$. This is the lateral pressure on a filament segment necessary to compress it axially and to create new smectic layers at the surface to conserve the volume. On the other hand, the pressure resulting from the surface tension can be approximated by $p_\mathrm{s} = \frac{\mathrm{d}A}{\mathrm{d}L}\frac{\sigma}{A_\mathrm{f}}$ with the front area $A_\mathrm{f} = V/L$.

The outer filament surface (neglecting the tip front area A_f for $L \gg R$) is $A = 2(\pi VL)^{1/2}$ as given above, thus $p_\mathrm{s} = -\sqrt{\frac{\pi L}{V}}\sigma$, and using $v_\mathrm{tip} = -\frac{\mathrm{d}L}{\mathrm{d}t} = 2\dot{R}L/R$, one obtains $p_\mathrm{d} = \frac{\gamma}{L}v_\mathrm{tip}$.

Setting $p_\mathrm{d} + p_\mathrm{s} = 0$, one finds

$$v_\mathrm{tip} = \sqrt{\frac{\pi}{V}}\frac{\sigma}{\gamma}L^{3/2}. \quad (6)$$

We introduce

$$\beta = \frac{1}{2}\sqrt{\frac{\pi L_0}{V}}\frac{\sigma}{\gamma} = \frac{\sigma}{2R_0\gamma}, \quad (7)$$

where L_0 and R_0 are the initial length and radius of the filament. After integrating eqn (6) using $\mathrm{d}L = -v_\mathrm{tip}\mathrm{d}t$, we obtain

$$L(t) = \frac{L_0}{(1+\beta t)^2} \quad (8)$$

$$v_\mathrm{tip}(t) = \frac{2\beta L_0}{(1+\beta t)^3} \quad (9)$$

In this model, we have assumed in the beginning that each filament segment moves at a constant speed, the capillary pressure and viscous stress compensate everywhere in the filament. In fact, the tip velocity decreases according to eqn (7), and so does the velocity of each segment. This means inertial forces have to be included in the pressure balance for a more accurate calculation. A linear pressure gradient, taking into account the pressure decrease along the filament axis, can be assumed as $\frac{\mathrm{d}p_i}{\mathrm{d}z}(t) = -\varrho\dot{v}(z)$, so $p_\mathrm{s} + p_\mathrm{d} = z\varrho\dot{v}_0\frac{z}{L}$, where z is a material-fixed coordinate which moves with the local filament. This yields a second order differential equation for L, which presumably can be solved only numerically. However, an order of magnitude analysis shows that p_s is of the order of $\sigma/R \approx 4000$ Pa, the term p_d is of the same order of magnitude. The deceleration adds a term of the order of $\varrho\dot{v}_0L$, which hardly exceeds 100 Pa. Accordingly, it is appropriate to neglect the inertial term and use eqn (8) to fit our experimental data. Indeed, we found that this function is well suited to fit all experimental data shown above. Since the number of waves was constant during retraction, $\lambda(t)$ has the same time dependence as $L(t)$ and we could well fit $\lambda(t)$ in Fig. 3(b) with an equation proportional to eqn (8). In Fig. 4, the measured z_tip was fitted by L_0–$L(t)$ with only one fit parameter β, while the initial length L_0 was set to the measured value. Good fits were obtained only in the initial phase of recoil, where eqn (8) is valid (thick lines). Thin lines correspond to the same fit equations and show how they deviate from the data outside the fit range. There, corrections due to flow into the meniscus *etc.* become essential.

The values of the relaxation rate β obtained by the fit are the following: Fig. 4(a) β(165 °C) = 185 s^{-1}, β(170 °C) = 66 s^{-1}; (b) β(160 °C) = 78 s^{-1}, β(165 °C) = 39 s^{-1}; (c) β(1.1 mm s^{-1}) = 17 s^{-1}; β(1.3 mm s^{-1}) = 33 s^{-1}; β(1.7 mm s^{-1}) = 131 s^{-1}; β(1.9 mm s^{-1}) = 351 s^{-1}; (d) β(1.1 mm s^{-1}) = 19 s^{-1}; β(1.3 mm s^{-1}) = 182 s^{-1}; β(1.7 mm s^{-1}) = 306 s^{-1}; β(1.9 mm s^{-1}) = 418 s^{-1}. The viscosity γ related to the permeation flow normal to the layers was calculated from the fit values of β as defined in eqn (7) by assuming a surface tension[40] σ = 25 mN m^{-1} and an average initial radius of the filaments R_0 = 3 μm (although R_0 may vary by a factor 2). The viscosity values obtained are the following: Fig. 4(a) γ(165 °C) = 23 Pa s, γ(170 °C) = 63 Pa s; Fig. 4(b) γ(160 °C) = 53 Pa s, γ(165 °C) = 107 Pa s; Fig. 4(c) γ(1.1 mm s^{-1}) = 245 Pa s; γ(1.3 mm s^{-1}) = 126 Pa s; γ(1.7 mm s^{-1}) = 31 Pa s; γ(1.9 mm s^{-1}) = 12 s^{-1}; Fig. 4(d) γ(1.1 mm s^{-1}) = 219 Pa s; γ(1.3 mm s^{-1}) = 23 Pa s; γ(1.7 mm s^{-1}) = 14 Pa s; γ(1.9 mm s^{-1}) = 10 Pa s. The lower range of viscosity values of 10–20 Pa s are in the same range as shear viscosity values measured previously on these and similar liquid crystals in the B_7 phase during shear flow.[38]

There are several interesting trends we can see on these viscosity values: (i) the viscosity values under the same conditions are larger for N16 (Fig. 4(b) and (d)) than for N7 (Fig. 4(a) and (c)). This is consistent with the smaller b values of N7 ($b \sim 9$ nm for N7 and $b \sim 16$ nm for N16 as seen in Fig. 1(a)), meaning more areas with lower packing densities[30] where the molecules can be

pushed between layers. (ii) The viscosities at higher temperatures appear to be lower. For N7 it is consistent with the slightly increasing b values toward higher temperatures, however, for N16 it is not the case indicating the role of other factors in determining the viscosity for permeation flows. (iii) The apparent viscosities are larger when the rupture occurred at higher pulling speeds. This indicates the annihilation of defects at higher pulling speeds leading to a decrease of the permeation sites, thus an increase of the apparent viscosity at higher pulling speeds.

Looking at Fig. 4, we can see that the fits consistently give up to 20–30% lower than measured recoil rates at the last stage of the recoil. This is related to the flow back to the meniscus that results in shorter $L(t)$, which was not considered in our model. Such a deviation is consistent with Fig. 3(a).

To summarize, the recoil processes of viscoelastic free-standing liquid crystal filaments are investigated experimentally and theoretically. The rupture starts with a buckling instability. During recoil the initial buckling pattern is affinely compressed with the retracting filament tip, and the total length of the filament slowly decreases. The shrinkage of the filament length is mainly compensated by its thickening, which dissipates the energy gain related to the decrease of the surface energy. A flow back into the meniscus is relevant only in the final stage of rupture. We introduced a theoretical model that takes into account the dissipation related to the thickening and explains the measured retraction speed quantitatively. The model opens new insights into the dynamics of smectic materials. It will be interesting to compare the results with filaments of simple smectic (A or C) phases to test how the permeation coefficient γ depends upon the phase structure. The problem is that such filaments are not stable, they can only be created during pinch-off processes or rupture of smectic films.[39]

Acknowledgements

This work was supported by the National Science Foundation under grants DMR No. 1307674, OISE 1259419 and DFG within grant STA 425/28.

References

1 J. Gladden, N. Handzy, A. Belmonte and E. Villermaux, *Phys. Rev. Lett.*, 2005, **94**, 035503.
2 R. Vermorel, N. Vandenberghe and E. Villermaux, *Proc. R. Soc. A*, 2007, **463**, 641–658.
3 C. Dombrowski, B. Lewellyn, A. I. Pesci, J. M. Restrepo, J. O. Kessler and R. E. Goldstein, *Phys. Rev. Lett.*, 2005, **95**, 184501.
4 M. Le Merrer, D. Quéré and C. Clanet, *Phys. Rev. Lett.*, 2012, **109**, 064502.
5 S. I. Nagahiro and Y. Hayakawa, *Phys. Rev. E: Stat., Nonlinear, Soft Matter Phys.*, 2008, **78**, 8–11.
6 Y. Rahmani, M. Habibi, A. Javadi and D. Bonn, *Phys. Rev. E: Stat., Nonlinear, Soft Matter Phys.*, 2011, **83**, 1–4.
7 N. M. Ribe, M. Habibi and D. Bonn, *Annu. Rev. Fluid Mech.*, 2012, **44**, 249–266.
8 W. S. Ryu and A. D. T. Samuel, *Nature*, 1998, **392**, 140.
9 L. Euler, *Opera Omnia I*, 1744, vol. 34, pp. 231–297.
10 H. E. Lindberg, *J. Appl. Mech.*, 1965, **32**, 315–322.
11 S. Alexander, *Phys. Rep.*, 1998, **65**, 236.
12 L. Golubovic, D. Moldovan and A. Peredera, *Phys. Rev. Lett.*, 1998, **81**, 3387.
13 C. W. Wolgemuth, T. R. Powers and R. E. Goldstein, *Phys. Rev. Lett.*, 2000, **84**, 1623–1626.
14 H. Fu, T. Powers and C. Wolgemuth, *Phys. Rev. Lett.*, 2007, **99**, 258101.
15 F. P. Gosselin, P. Neetzow and M. Paak, *Phys. Rev. E: Stat., Nonlinear, Soft Matter Phys.*, 2014, **90**, 052718.
16 F. Vollrath and D. P. Knight, *Nature*, 2001, **410**, 541–548.
17 D. K. Vig and C. W. Wolgemuth, *Phys. Rev. Lett.*, 2012, **109**, 218104.
18 A. A. Evans, S. E. Spagnolie, D. Bartolo and E. Lauga, *Soft Matter*, 2013, **9**, 1711.
19 M. R. Rehorn, A. K. Schroer and S. S. Blemker, *J. Biomech.*, 2014, **47**, 687–693.
20 L. Rayleigh, *Proc. London Math. Soc.*, 1879, **10**, 4–13.
21 L. Rayleigh, *Proc. London Math. Soc.*, 1878, **XI**, 50–57.
22 A. Jákli and A. Saupe, *One and Two Dimensional Fluids – Physical Properties of Smectic Lamellar and Columnar Liquid Crystals*, Taylor & Francis, Boca Raton, 2006.
23 C. A. Bailey, M. Murphy, A. Eremin, W. Weissflog and A. Jákli, *Phys. Rev. E: Stat., Nonlinear, Soft Matter Phys.*, 2010, **81**, 031708.
24 J. Petzold, A. Nemeș, A. Eremin, C. Bailey, N. Diorio, A. Jákli, R. Stannarius and A. Nemes, *Soft Matter*, 2009, **5**, 3120–3126.
25 R. Stannarius, A. Nemeş and A. Eremin, *Phys. Rev. E: Stat., Nonlinear, Soft Matter Phys.*, 2005, **72**, 020702.
26 A. Nemeş, A. Eremin, R. Stannarius, M. Schulz, H. Nádasi and W. Weissflog, *Phys. Chem. Chem. Phys.*, 2006, **8**, 469–476.
27 T. Ostapenko, S. M. Salili, A. Eremin, A. Jákli and R. Stannarius, *Ferroelectrics*, 2014, **468**, 101–113.
28 A. Jákli, D. Krüerke and G. G. Nair, *Phys. Rev. E: Stat., Nonlinear, Soft Matter Phys.*, 2003, **67**, 051702.
29 G. Pelzl, S. Diele, A. Jákli, C. H. Lischka, I. Wirth and W. Weissflog, *Liq. Cryst.*, 1999, **26**, 135–139.
30 C. Zhang, S. M. Salili, N. Diorio, W. Weissflog and A. Jákli, *Liq. Cryst.*, 2015, **42**, 1621–1626.
31 N. Vaupotič, M. Čopič, E. Gorecka and D. Pociecha, *Phys. Rev. Lett.*, 2007, **98**, 247802.
32 C. Folcia, J. Etxebarria, J. Ortega and M. B. Ros, *Phys. Rev. E: Stat., Nonlinear, Soft Matter Phys.*, 2005, **72**, 041709.
33 S. G. Taylor, *Proc. R. Soc. A*, 1959, **253**, 313–321.
34 F. E. C. Culick, *J. Appl. Phys.*, 1960, **31**, 1128–1129.
35 G. Debrégeas, P. Martin and F. Brochart-Wyart, *Phys. Rev. Lett.*, 1995, **75**, 3886.
36 A. Eremin, *et al.*, *Phys. Rev. Lett.*, 2012, **109**, 017801.
37 D. A. Coleman, *et al.*, *Science*, 2003, **301**, 1204.
38 C. A. Bailey, K. Fodor-Csorba, J. T. Gleeson, S. N. Sprunt and A. Jákli, *Soft Matter*, 2009, **5**, 3618.
39 K. May, K. Harth, T. Trittel and R. Stannarius, *ChemPhysChem*, 2014, **15**, 1508.
40 See, *e.g.* H. Schüring, C. Thieme and R. Stannarius, *Liq. Cryst.*, 2001, **28**, 241.

